



Swansea University
Prifysgol Abertawe



Cronfa - Swansea University Open Access Repository

This is an author produced version of a paper published in:
ACS Nano

Cronfa URL for this paper:
<http://cronfa.swan.ac.uk/Record/cronfa50476>

Paper:

Hocevar, S., Milosevic, A., Rodriguez-Lorenzo, L., Ackermann-Hirschi, L., Mottas, I., Petri-Fink, A., Rothen-Rutishauser, B., Bourquin, C. & Clift, M. (in press). Polymer-coated gold nanospheres do not impair the innate immune function of human B lymphocytes in vitro. *ACS Nano*

This item is brought to you by Swansea University. Any person downloading material is agreeing to abide by the terms of the repository licence. Copies of full text items may be used or reproduced in any format or medium, without prior permission for personal research or study, educational or non-commercial purposes only. The copyright for any work remains with the original author unless otherwise specified. The full-text must not be sold in any format or medium without the formal permission of the copyright holder.

Permission for multiple reproductions should be obtained from the original author.

Authors are personally responsible for adhering to copyright and publisher restrictions when uploading content to the repository.

<http://www.swansea.ac.uk/library/researchsupport/ris-support/>

This document is confidential and is proprietary to the American Chemical Society and its authors. Do not copy or disclose without written permission. If you have received this item in error, notify the sender and delete all copies.

Polymer-Coated Gold Nanospheres Do Not Impair the Innate Immune Function of Human B Lymphocytes *In Vitro*

| | |
|-------------------------------|--|
| Journal: | ACS Nano |
| Manuscript ID | nn-2019-01492f.R1 |
| Manuscript Type: | Article |
| Date Submitted by the Author: | n/a |
| Complete List of Authors: | Hočevar, Sandra; University of Geneva, Milošević, Ana ; Adolphe Merkle Institute Rodriguez-Lorenzo, Laura; Adolphe Merkle Institute Ackermann-Hirschi, Liliane ; Adolphe Merkle Institute Mottas, Ines; University of Geneva Petri-Fink, Alke; Adolphe Merkle Institute Rothen-Rutishauser, Barbara; Adolphe Merkle Institute Bourquin, Carole; University of Geneva Clift, Martin; Swansea University, College of Medicine |
| | |

SCHOLARONE™
Manuscripts

1
2
3
4
5
6
7
8
9
10
11
12
13
14
15
16
17
18
19
20
21
22
23
24
25
26
27
28
29
30
31
32
33
34
35
36
37
38
39
40
41
42
43
44
45
46
47
48
49
50
51
52
53
54
55
56
57
58
59
60

Polymer-Coated Gold Nanospheres Do Not Impair the Innate Immune Function of Human B Lymphocytes *In Vitro*

Sandra Hočevar^{1,2}, *Ana Milošević*^{1,†}, *Laura Rodriguez-Lorenzo*^{1,§}, *Liliane Ackermann-Hirschi*¹, *Ines Mottas*^{2,3}, *Alke Petri-Fink*¹, *Barbara Rothen-Rutishauser*¹, *Carole Bourquin*^{2,3,4,*}, *Martin J. D. Clift*^{1,5,*}

¹BioNanomaterials, Adolphe Merkle Institute, University of Fribourg, 1700 Fribourg, Switzerland.

²School of Pharmaceutical Sciences, University of Geneva, University of Lausanne, 1211 Geneva, Switzerland

³Chair of Pharmacology, Faculty of Science and Medicine, University of Fribourg, 1700 Fribourg, Switzerland

⁴Faculty of Medicine, University of Geneva, Rue Michel-Servet 1, 1211 Geneva, Switzerland

⁵*In Vitro* Toxicology Group, Swansea University Medical School, Wales, SA2 8PP, UK

1
2
3 ABSTRACT
4
5
6

7 Gold nanoparticles (GNPs) are intended for use within a variety of biomedical applications due
8 to their physicochemical properties. Although, in general, biocompatibility of GNPs with
9 immune cells such as macrophages and dendritic cells is well established, the impact of GNPs
10 on B lymphocyte immune function remains to be determined. Since B lymphocytes play an
11 important role in health and disease, the suitability of GNPs as a B cell-targeting tool is of high
12 relevance. Thus, we provide information on the interactions of GNPs with B lymphocytes.
13 Herein, we exposed freshly isolated human B lymphocytes to a set of well-characterized and
14 biomedically relevant GNPs with distinct surface (polyethylene glycol (PEG), PEG/polyvinyl
15 alcohol (PEG/PVA)) and shape (spheres, rods) characteristics. Polymer-coated GNPs poorly
16 interacted with B lymphocytes, in contrast to uncoated GNPs. Importantly, none of the GNPs
17 significantly affected cell viability, even at the highest concentration of 20 $\mu\text{g}/\text{ml}$ over a 24 h
18 suspension exposure period. Furthermore, none of the nanosphere formulations affected the
19 expression of activation markers (CD69, CD86, MHC II) of the naïve B lymphocytes, nor did
20 they cause an increase in the secretion of pro-inflammatory cytokines (i.e., IL-6, IL-1 β).
21 However, the absence of polymer coating on the sphere GNPs and the rod shape caused a
22 decrease in IL-6 cytokine production by activated B lymphocytes, suggesting a functional
23 impairment. With these findings, the present study contributes imperative knowledge towards
24 the safe-by-design approaches being conducted to benefit the development of nanomaterials,
25 specifically those as theranostic tools.
26
27
28
29
30
31
32
33
34
35
36
37
38
39
40
41
42
43
44
45
46
47
48
49
50

51
52 **KEYWORDS:** gold nanoparticles, B lymphocytes, nanotoxicology, innate immunity, antigen
53 presenting cells
54
55
56
57
58
59
60

1
2
3 B lymphocytes, often referred to as B cells, are an important sub-population of immune cells
4 that are found throughout the body in the blood and lymphoid organs. As the sole producers of
5 antibodies, they are essential effectors of protective immunity against infections. B cells also
6 regulate the function of other immune cells, such as T lymphocytes, by presenting processed
7 antigens *via* the major histocompatibility complex (MHC) and by secreting various cytokines
8 that act as immune mediators. In pathological conditions, B cell dysfunction can lead to diseases
9 such as allergy, autoimmunity or cancer.¹ Because of their critical role in health and disease, B
10 cells have generated increased interest in recent years as a target for drug delivery. Indeed, B
11 cells have been successfully targeted by 80 nm lipid nanoparticles (NPs) carrying vaccines
12 against influenza, HIV or Zika virus, or immunotherapies against allergic diseases.²⁻⁴ Despite
13 these recent advances, the direct impact of NPs on B lymphocytes is still poorly understood.
14 Importantly, B cells can respond in an innate, antigen-independent manner to different stimuli
15 following activation *via* conserved pattern-recognition receptors, *i.e.* Toll-like receptors. This
16 initial innate stimulation critically modulates subsequent activation and differentiation of B
17 cells.⁵ Thus, in consideration of the human health impact of exposure to NPs it is imperative to
18 understand how NPs may affect B cells, including their possible cytotoxic profile, as well as
19 their ability to modulate their innate immune function.
20
21
22
23
24
25
26
27
28
29
30
31
32
33
34
35
36
37
38
39
40

41
42 The immunotoxicity of NPs has, to date, been studied essentially upon myeloid immune cells
43 such as macrophages and dendritic cells. The phagocytotic nature of these cells leads to
44 engulfment of the NPs, which in turn can promote interference with immune functions.⁶ Thus,
45 some types of NPs (*e.g.*, carbon nanotubes, zinc oxide and silica NPs) can cause dysfunctions
46 in cell-intrinsic mechanisms such as autophagy and increases in secretion of pro-inflammatory
47 cytokines, which consequentially may trigger oxidative stress and potentially genotoxicity.⁷⁻⁹
48 To minimize the potential toxicity of NPs and to improve their half-life in the body, NP surface
49 functionalization integrated with protective polymer surface coatings are used. Polyethylene
50
51
52
53
54
55
56
57
58
59
60

glycol (PEG) and polyvinyl alcohol (PVA) as well as their co-polymer formulation are commonly used as protectors in cosmetic products, food supplements and pharmaceuticals.^{10,11} However, use of these polymer coatings for NPs designed for therapeutic applications also has undesired effects: it may lead to the production of anti-polymer antibodies, which cause NP opsonization. This then increases clearance of the NPs and therefore affects the efficacy of treatment.¹² To better evaluate the safety of the NPs for the immune system as a whole therefore, it is important to understand distinct effects that NPs may have on different immune subsets. Moreover, direct impact of NPs on B lymphocytes is currently a significant knowledge gap in the field, evidenced by the limited literature on the topic.

Among the variety of nanomaterials available, gold core-based nanoparticles (GNPs) are frequently used as nanomedical tools in therapy, diagnostics and drug delivery. The optical properties of GNPs and their high biocompatibility make them highly useful imaging tools, biosensors, and nanocarriers.¹³ Furthermore, GNPs efficiently deliver vaccines and immunotherapies to immune cells, achieving effective immune responses with low amounts of cargo.^{14,15} In view of the emerging strategies to target B lymphocytes with nanocarriers, and the lack of information about NP immunotoxicity on B cells, we have investigated here the impact of a set of well-characterized GNPs on the phenotype and function of freshly isolated CD20⁺ human B lymphocytes from peripheral blood.

RESULTS

GNPs with different polymer coatings and shapes were observed to be stable in a biological environment. To examine the impact of GNPs on B lymphocytes, we selected a panel of GNPs with different functionalizations and shapes that have previously been well characterized. Specifically, these were citrate-stabilized gold nanospheres (citrate-GNS) and polymer-functionalized gold nanospheres coated either with PEG (PEG-GNS) or a combination

1
2
3 of PEG and PVA (PEG/PVA-GNS), as well as PEGylated gold nanorods (PEG-GNR).^{16,17} Gold
4 core diameters were measured by transmission electron microscopy (TEM) as 13.4 ± 2.3 ,
5
6 15.7 ± 1.9 and 14.6 ± 1.8 nm for citrate-GNS, PEG-GNS and PEG/PVA-GNS, respectively.
7
8
9 Dimensions of the PEG-GNR were measured at 57 ± 12 nm x 15 ± 3 nm, giving the aspect ratio
10
11 of 3 ± 0.8 (Figure. 1A and Table 1).
12
13

14
15 UV-Vis measurements confirmed the stability in H₂O of all GNPs, as previously described
16
17 (Figure 1B).¹⁸ Since biological media can affect NP colloidal stability,^{19,20} GNPs were
18
19 incubated for 24 h at 37° C, 5% CO₂ in complete cell culture media supplemented with 10%
20
21 human plasma (Roswell Park Memorial Institute 1640 medium + human plasma (RPMI+HP))
22
23 or in PBS. A loss in stability was observed for citrate-GNS due to aggregation in culture media,
24
25 as previously described.²¹ Complete aggregation of citrate-GNS was present in PBS (Figure
26
27 1B). In contrast, no signs of increased colloidal instability were detected for either type of
28
29 polymer-coated GNS or the PEG-GNR.
30
31
32

33
34 To further examine their colloidal stability, the hydrodynamic diameter of GNPs in biological
35
36 media was characterized (Table 1). Negatively charged, non-polymer coated, citrate-stabilized
37
38 NPs are known to interact strongly with a protein-rich environment, leading to a change in
39
40 hydrodynamic diameter due to the formation of a protein corona.²²⁻²⁴ Indeed, dynamic
41
42 depolarized light scattering (DDLS) results showed a strong increase in citrate-GNS diameter
43
44 in RPMI+HP compared to H₂O. For polymer-coated GNPs, the radius did not change in cell
45
46 culture media, suggesting that a high-density PEG or PEG/PVA coating of the GNPs prevented
47
48 surface protein absorption.²⁵ In addition, PEG-GNR were tested for the efficiency of PEG
49
50 coverage in relation to cetyltrimethylammonium bromide (CTAB) residues that might be still
51
52 present from the synthesis. The results shown in Table 1 reveal that PEGylated GNRs presented
53
54 higher hydrodynamic radii than the as-synthesized GNRs: 34.8 ± 0.2 nm vs. 20.7 ± 0.3 nm. The
55
56 surface grafted PEG chains can acquire either a “brush” or “mushroom” conformation. The
57
58
59
60

1
2
3 latter mainly occurs when the attachment distance of PEG to the surface (D) is larger than the
4
5 Flory radius (R_F), while the brush conformation is observed when D is smaller than R_F .²⁶
6
7 PEGylated GNRs presented a grafting coverage of 0.22 PEG molecules per nm^2 and D of 2.26
8
9 nm, as obtained by a method previously described.²⁷ This indicated that the PEG layers
10
11 deposited on the GNRs possessed a brush-like conformation because the R_F for 5,000 Da PEG
12
13 is 4.9 nm. This allowed us to conclude that no potential interference of otherwise toxic CTAB²⁸
14
15 remained on the surface of the GNRs.²⁹
16
17
18

19 The significance of the NP surface charge and the role that it plays in the NP-cell interface is
20
21 frequently stressed.^{30,31} We assessed the effect of the biological environment on the surface
22
23 charge of GNPs and found that the charge of citrate-GNS considerably changed in RPMI+HP
24
25 compared to H_2O , most likely due to the surface adsorption of the plasma protein.^{32,33} In
26
27 contrast, polymer-coated GNPs presented a slightly negative charge in both H_2O and RPMI+HP
28
29 with no major change (Table 1). This confirms that surface charge can vary significantly
30
31 depending on the GNP surface chemistry, therefore, well-designed polymer functionalization
32
33 is needed in order to avoid unwanted interactions of GNP with biological media.
34
35
36
37
38
39
40
41
42
43
44
45
46
47
48
49
50
51
52
53
54
55
56
57
58
59
60

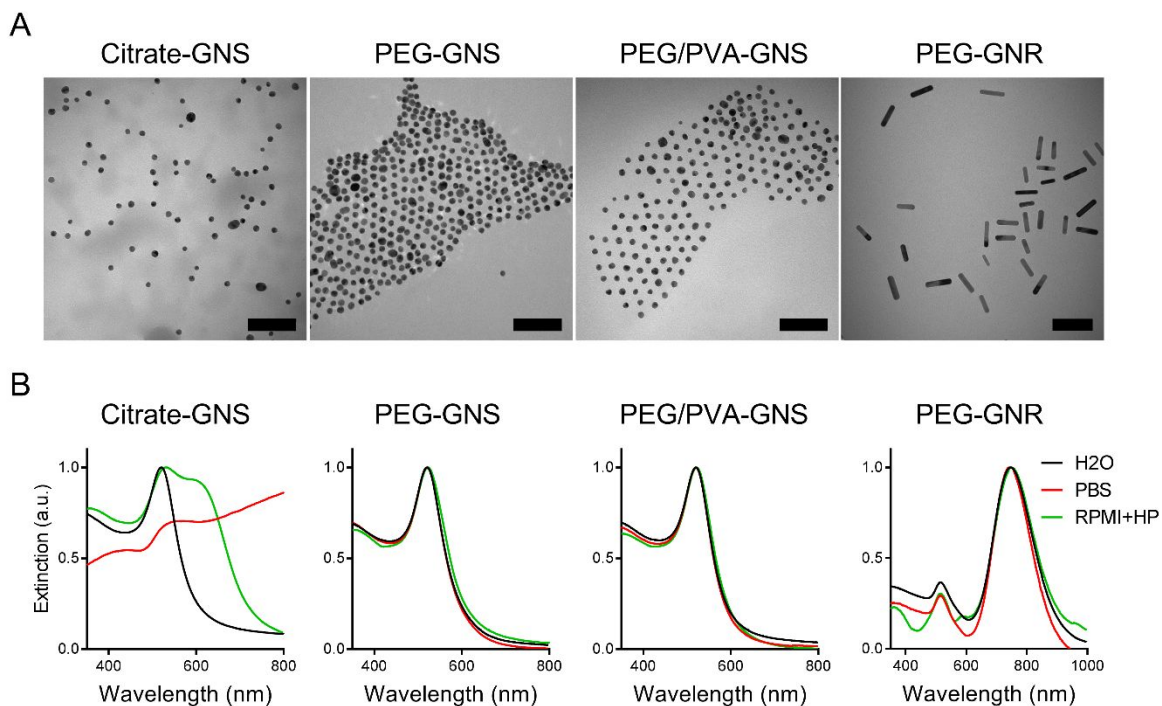


Figure 1. Characterization of gold nanoparticles (GNPs). (A) Representative TEM images of citrate-stabilized gold nanospheres (Citrate-GNS), gold nanospheres with a polyethylene glycol polymer coating (PEG-GNS), gold nanospheres with a combination of PEG and PVA polymer coating (PEG/PVA-GNS), and gold nanorods with PEG coating (PEG-GNR) in H₂O. Scale bars: 100 nm. (B) UV-Vis spectra of GNPs in different biological media. Each spectrum was normalized relative to their maximum wavelength. RPMI+HP: complete culture medium consisting of Roswell Park Memorial Institute 1640 with 1% Penicillin/Streptomycin, 1% L-Glutamine and 10% human plasma.

Table 1. Characterization of gold nanoparticle size and surface charge in complete culture medium, phosphate buffered saline (PBS) and water (H₂O).

| | Size (nm) | | | ζ-potential (mV) | | |
|--------------------|------------------------------|------------------|----------|------------------|------------|----------|
| | TEM (d_c) | DDLS (d_h) | | H ₂ O | PBS | RPMI+HP |
| | | H ₂ O | RPMI+HP | | | |
| Citrate-GNS | 13.4±2.3 | 16.8±0.1 | 48.0±0.5 | -34.7±1.0 | Aggregated | -9.7±2.1 |
| PEG-GNS | 15.7±1.9 | 26.8±0.3 | 27.1±0.2 | -5.8±1.3 | -6.8±0.8 | -7.4±1.4 |
| PEG/PVA-GNS | 14.6±1.8 | 23.7±0.8 | 25.5±1.6 | -6.5±0.9 | -13.7±0.9 | -8.9±1.6 |
| PEG-GNR | Length: 57±12 Width: 15±3 | 34.8±0.2 | 33.9±0.3 | -13.6±1.5 | -3.4±1.7 | -9.9±2.9 |
| GNR | n/a | 20.7±0.3 | n/a | n/a | n/a | n/a |

d_c : core diameter, d_h : hydrodynamic diameter, RPMI+HP: complete culture medium consisting of Roswell Park Memorial Institute 1640 with 1% Penicillin/Streptomycin, 1% L-Glutamine and 10% human plasma.

GNPs do not affect B lymphocyte viability. The biological impact of GNPs on immune cells varies according to their physicochemical properties. Several groups have shown that characteristics such as size, shape and polymer coating affect the toxicity of GNPs on macrophages and dendritic cells.^{34–36} To assess whether the GNPs described above impact B lymphocyte viability, total CD20⁺ human B lymphocytes were freshly isolated from the blood of healthy donors and exposed to increasing concentrations of GNPs. This cell population consists mainly of naïve B cells (65-75%), with 20-25% memory B cells.³⁷ A 24 h exposure time was selected in order to detect early B-cell responses toward GNPs. Then, cells were stained with amine-reactive fluorescent viability dye (Zombie NIR) and analyzed by flow cytometry. The polymer-functionalized GNS (PEG and PEG/PVA) as well as citrate-GNS caused no significant cell death at concentrations up to 20 µg/ml (Figure 2A). PEG-GNRs, studied at the highest concentration of 20 µg/ml only, also did not impact B cell viability. This latter finding demonstrating that neither the type of polymer coating nor geometry impacts upon B cell viability following GNP exposure (Figure 2B). In addition, phase contrast images did not

show decrease in B cell density nor a change in cell morphology upon 24h GNP exposure (Figure S1A).

The small molecule R848 has been reported as an antigen-independent immune activator and stimulator of B lymphocyte proliferation by signaling *via* the receptor TLR7.^{38,39} Importantly, B cell viability was not compromised following exposure to GNPs together with the stimulant, irrespective of their shape or functionalization (Figure 2).

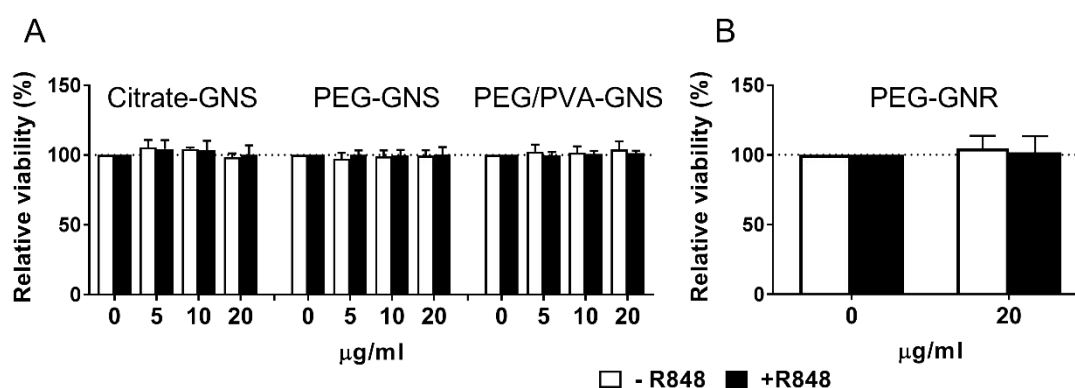


Figure 2. GNPs do not impact upon B lymphocyte viability. Viability of human B lymphocytes was determined by staining cells with Zombie NIR viability dye (1:1000) and measured by flow cytometry after 24 h exposure to GNS (5-20 µg/ml) with different surface functionalizations (A) or to PEG-GNR (20 µg/ml) (B). Cells were incubated with and without the immunostimulant R848 (2 µg/ml). Data are presented relative to control cells without GNP exposure (=100%). Data represent mean \pm SD of three separate experiments on different donors (n=3). Data were assessed by a two-way ANOVA, followed by Tukey's multiple comparison *post-hoc* test. The alpha value was set at 0.05.

1
2
3 **Citrate-GNPs are taken up by B lymphocytes, but not polymer-coated GNPs.** B
4
5 lymphocytes are professional antigen-presenting cells and as such they have the ability to take
6
7 up pathogens, in particular *via* B cell receptor-mediated endocytosis.⁴⁰ To examine whether B
8
9 lymphocytes could take up GNP, freshly isolated human B cells were exposed to GNPs for 24
10
11 h. The highest GNP concentration tested (20 $\mu\text{g}/\text{ml}$) was considered to be in the sub-lethal range
12
13 as it did not cause significant B cell death. Therefore, it was further used in NP-cell association
14
15 experiments. Macrophages and dendritic cells are professional phagocytotic cells and known to
16
17 easily take up NPs.⁴¹ Therefore, human monocytes-derived macrophages (MDMs) and
18
19 monocyte-derived dendritic cells (MDDCs) were also exposed to the previously described
20
21 GNPs under the same conditions as the B cell experiments. MDMs and MDDCs served as a
22
23 control for GNP-B cell interaction as well as for comparison of GNP-B cell association across
24
25 different APC types.
26
27
28
29

30
31 The cells and the GNP uptake were first visualized by dark field hyperspectral imaging (DF-
32
33 HSI) coupled with fluorescent detection. For citrate-GNS, which were noted to readily
34
35 aggregate in biological media, clusters of NPs were clearly visible on the surface of B cells
36
37 (Figure 3A). The particles were also detectable within the B cells themselves (insert Figure 3A).
38
39 Citrate-GNS were further observed to be internalized by MDMs and MDDCs, as expected for
40
41 these highly phagocytotic cell types (Figure 3A and Figure S1B and S1C). In contrast to citrate-
42
43 stabilized GNS, no interaction (either internalization or cell surface association) of polymer-
44
45 coated GNS with B lymphocytes was detected by DF-HSI. Similarly, PEG-GNR did not show
46
47 any association with B cells (Figure S3). In MDMs, only a few intracellular aggregates of PEG-
48
49 GNS and PEG/PVA-GNS were detected by DF-HSI (Figure 3A).
50
51
52
53

54 A subsequent approach to determine NP internalization by mammalian cells is through
55
56 changes in light scattering detected by flow cytometry. This was previously reported by Zucker
57
58 et al.,⁴² who demonstrated that the internalization of TiO_2 NPs increased side scatter (SSC) and
59
60

1
2
3 decreased forward scatter (FSC) by epithelial cells. An increase in SSC was observed for B
4
5 cells exposed to citrate-GNS, but not to polymer-coated GNS (Figure S4). In contrast, in MDMs
6
7 and MDCCs, an increase in side scatter was observed for polymer-coated GNS. Overall, these
8
9 results supported the observations collected from the DF-HSI images.

10
11
12 To quantify the uptake of GNPs with human B cells and to compare this to the association by
13
14 other APCs, we measured the gold content within B cells and MDMs after exposure to 20 $\mu\text{g/ml}$
15
16 of GNPs by using inductively coupled plasma mass spectroscopy (ICP-MS). This technique
17
18 allows precise quantification of the gold ion content in biological samples.⁴³ The uptake of
19
20 citrate-GNS by B cells was confirmed, with approximately 10 μg gold measured per 10^6 cells
21
22 (calculated by dividing measured GNP mass per total cell count and multiplying by 10^6) (Figure
23
24 3B). This corresponds to approximately 1% GNP-B cell association, as a function of measured
25
26 GNP mass per total exposed GNP mass. In contrast, polymer-coated GNPs were detected at
27
28 very low levels in B lymphocytes, confirming the findings obtained by DF-HSI. In comparison
29
30 to B cells, MDMs internalized polymer-coated GNPs approximately 10 times more efficiently.
31
32 Similar to B cells, citrate-GNS associated with MDMs with high efficiency compared to the
33
34 polymer-coated GNS (Figure 3B).

35
36
37 Here we demonstrate using DF-HSI that primary human B lymphocytes can internalize
38
39 aggregated citrate-GNPs. This in accordance with a previous report in a mouse B cell line of
40
41 the uptake of citrate GNPs aggregates, visualized in the endosomal compartments.⁴⁴ Clearly, as
42
43 shown in the present study, PEG-containing polymer coating prevents the uptake of the GNP
44
45 both in B cells and in myeloid cells such as macrophages and dendritic cells. This agrees with
46
47 previous results in dendritic cells, where GNPs coated with the combination of PEG/PVA had
48
49 a significantly lower uptake than with PVA coating alone, presumably due to the shielding role
50
51 of PEG.¹⁶ Our current results suggest that shape does not have a significant effect upon the
52
53 uptake by either B cells or macrophages and dendritic cells. Nevertheless, the exact mechanisms
54
55
56
57
58
59
60

and possible surface receptors involved in the GNP uptake by B lymphocytes across different physiochemical properties of GNPs remain unknown.

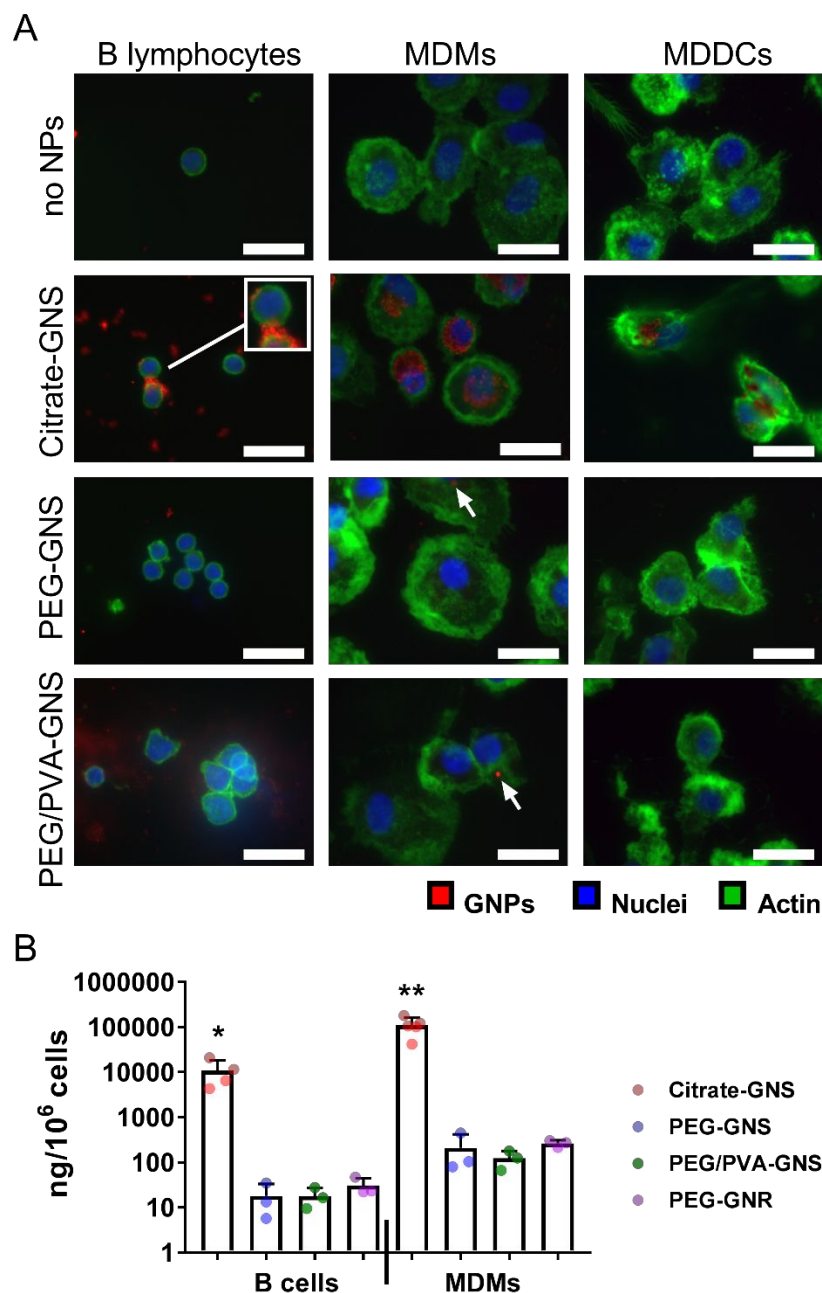


Figure 3. Polymer-coated GNPs cause limited B lymphocyte uptake. **(A)** Dark field hyperspectral images of B cells and other antigen-presenting cells exposed to GNS at 20 $\mu\text{g/ml}$ for 24 h. Scale bars: 5 μm . The white arrows indicate intracellular GNS. **(B)** Quantification by ICP-MS of gold ion content in B lymphocytes and MDMs exposed to GNPs at 20 $\mu\text{g/ml}$ for 24 h. Each dot represents one biological sample. Bars represent the mean \pm SD of 3-4 biological

1
2
3 replicates; * $p < 0.05$, ** $p < 0.01$. Data were evaluated by a one-way ANOVA, followed by
4
5 Tukey's multiple comparison *post-hoc* test.
6
7
8
9

10 **GNPs do not impair B lymphocyte activation.** Since gold-based nanoparticles have been
11 shown in some instances to stimulate B cell lines,⁴⁵ we investigated whether the GNPs used in
12 this study could lead to antigen-independent activation of primary human B cells. The immune
13 cell activation markers CD69, CD86 and MHC II were assessed on B cells by flow cytometry
14 after exposure of the cells to GNPs. The TLR7 ligand R848 was used as positive control for
15 antigen-independent B-cell activation.⁴⁶ In the absence of R848, expression of activation
16 markers was not increased after exposure to any of the tested GNS at concentrations up to 20
17 $\mu\text{g/ml}$ for 24 h (Figure 4A). Upon R848 stimulation, B cells showed upregulation of all three
18 activation markers, as expected. Importantly, exposure to GNS did not impair the
19 pharmacological activation of B cells by R848. Similar results were obtained for PEG-GNRs
20 at 20 $\mu\text{g/ml}$, which neither activated B cells nor inhibited their stimulation by R848 (Figure
21 4B). The activation status of MDMs and MDDCs exposed to GNS was also assessed: the
22 nanospheres did not activate these cells nor did they impair their stimulation by R848 (Figure
23 S6). Thus, the GNPs used in this study did not stimulate human B cells, and they did not
24 interfere with their drug-induced activation.
25
26
27
28
29
30
31
32
33
34
35
36
37
38
39
40
41
42
43
44
45
46
47
48
49
50
51
52
53
54
55
56
57
58
59
60

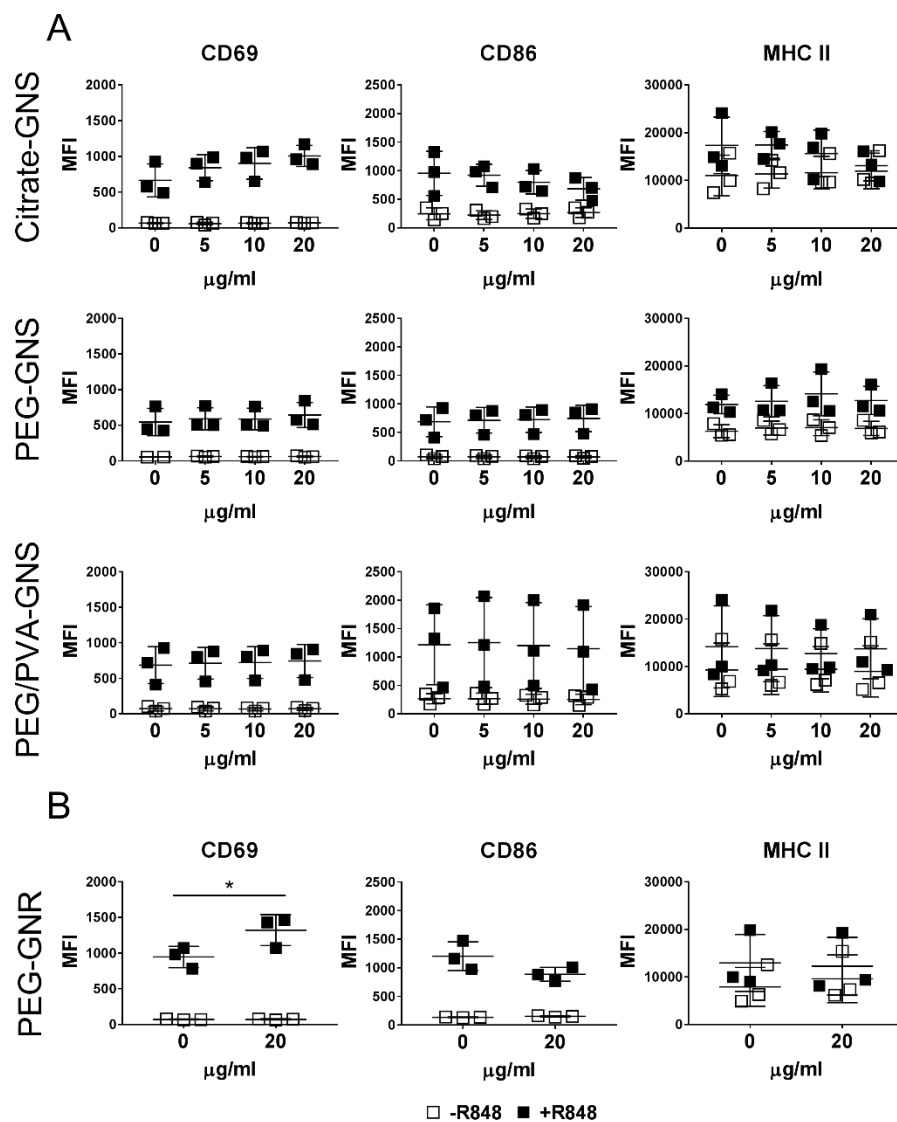


Figure 4. B lymphocyte activation. Surface activation markers on B lymphocytes (CD69, CD86 and MHC-II) measured by flow cytometry after 24 h exposure of B cells to GNS (5-20 $\mu\text{g/ml}$) with different surface functionalization (**A**) or to PEG-GNR (20 $\mu\text{g/ml}$) (**B**). B cells were incubated with or without the immunostimulant R848 (2 $\mu\text{g/ml}$). Each point represents one donor ($n=3$). Error bars: mean \pm SD; $*p<0.05$. Data were evaluated by a two-way ANOVA, followed by Tukey's multiple comparison *post-hoc* test. The alpha value was set at 0.05.

1
2
3 **Pro-inflammatory responses are not enhanced by GNPs.** Nanoparticles have been shown
4 to induce the production of pro-inflammatory mediators in immune cells.⁴⁷ In particular,
5 nanoparticles have been noted as able to trigger activation of the inflammasome complex, which
6 leads to the secretion of pro-inflammatory cytokines such as IL1 β .⁴⁸ Since inflammation can
7 result in severe side effects in patients, it is essential to test the pro-inflammatory potential of
8 NPs destined for biomedical applications early in their development process. To assess whether
9 GNPs induced the production of pro-inflammatory mediators in B cells, we measured the
10 secretion of the pro-inflammatory cytokines IL-6 and IL-1 β by B cells after a 24 h incubation
11 with GNPs, with or without R848. The levels of cytokines were determined by ELISA in the
12 cell culture supernatant. IL-6 and IL-1 β secretion was not induced by GNS at concentrations
13 up to 20 $\mu\text{g/ml}$, regardless of their functionalization, nor by PEG-GNR (Figure 5A). R848
14 stimulation induced production of both IL-6 and IL1 β by B cells, as expected for a TLR7
15 agonist, but this cytokine production was not affected by polymer-coated GNS. Interestingly,
16 PEG-GNR at 20 $\mu\text{g/ml}$ caused a significant drop in IL-6 concentration from otherwise increased
17 IL-6 levels of B cells induced by R848 (Figure 5B). Similarly, citrate-GNS caused suppression
18 of IL-6 production in R848-activated cells in a concentration-dependent fashion, although the
19 decrease was not statistically significant due to high variation between the cells from the
20 different donors.

21
22
23
24
25
26
27
28
29
30
31
32
33
34
35
36
37
38
39
40
41
42
43
44
45 In order to further compare the effect of GNPs across APCs, pro-inflammatory cytokines of
46 MDMs and MDDCs were measured after exposure to all types of GNS at the highest
47 concentration only (20 $\mu\text{g/ml}$). Similarly to B cells, none of GNS alone induced cytokine
48 release. Interestingly, citrate-GNS did not interfere with efficiency of the cytokine release by
49 MDMs and MDDCs, in contrast to the observations for activated B lymphocytes (Figure S7).

50
51
52
53
54
55
56
57
58
59
60
The potential interference of GNPs, which possess light-absorbing properties, with optical-
based assays such as ELISA must be considered. To exclude such an interference, we carefully

assessed potential background caused by GNPs alone in the optical signal of the plate reader and found that all GNPs, even at the highest concentration of 20 $\mu\text{g/ml}$, were below the detection level of the ELISA (data not shown). Further, we controlled for the possible absorbance of cytokines onto the surface of the GNPs, which could impact upon the reliable reading of cytokine concentrations *via* this method. We detected no effect of the GNPs on cytokine concentrations in this cell-free assay (Figure S8).

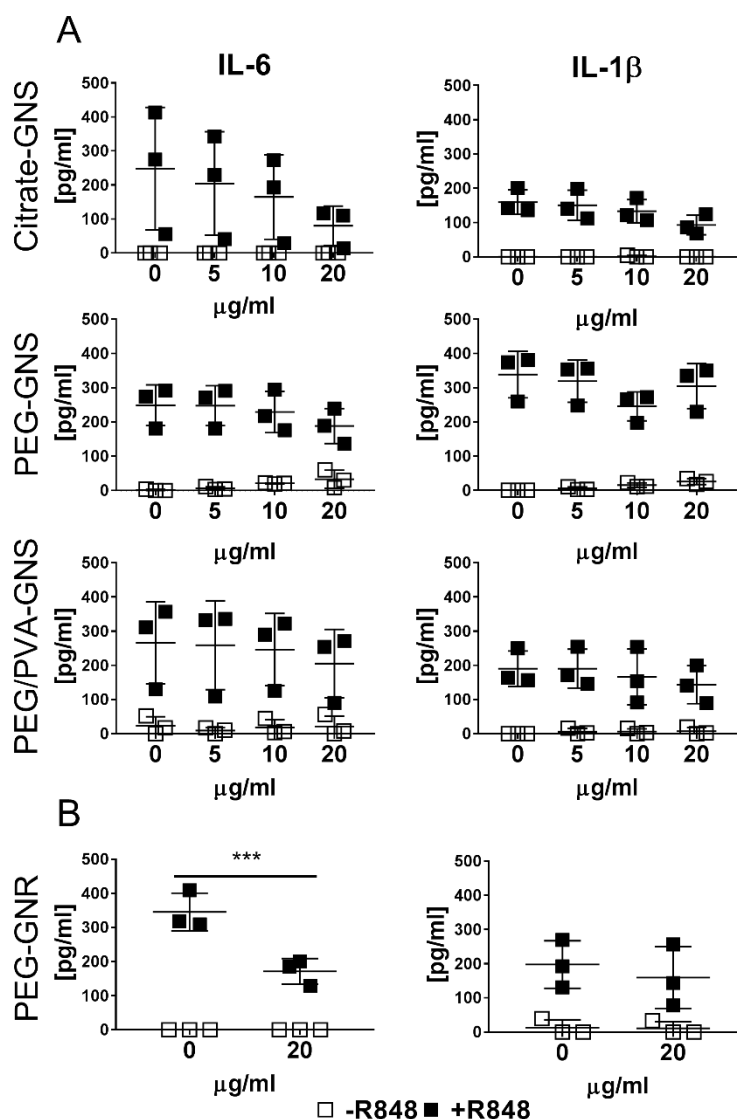


Figure 5. B lymphocyte pro-inflammatory response. Release of pro-inflammatory cytokines after 24 h exposure of B cells to GNS (5-20 $\mu\text{g/ml}$) with different surface functionalization (A) or to PEG-GNR (20 $\mu\text{g/ml}$) (B). B cells were incubated with or without the immunostimulant

1
2
3 R848 (2 $\mu\text{g/ml}$). Each point represents one donor ($n=3$). Error bars: mean \pm SD; *** $p<0.001$.

4
5 Data were evaluated by a two-way ANOVA, followed by Tukey's multiple comparison *post-*
6
7 *hoc* test. The alpha value was set at 0.05.
8
9

10 11 12 13 DISCUSSION

14
15
16
17 The interactions of GNPs with B lymphocytes are important for biomedical applications,
18 especially in view of the selective targeting of B lymphocytes by NPs. Although B lymphocytes
19 are generally not considered professional phagocytic cells, they are capable of, in theory,
20 actively taking up large particulate material through B-cell and complement receptors.⁴⁹ Our
21 results confirmed that GNPs which have a polymer-protected surface trigger very low uptake
22 by primary human B lymphocytes. In contrast, uncoated GNPs, which were opsonized by
23 plasma proteins, were highly taken up even by naïve B cells. This heightened interaction may
24 be due, in part, to the formation of NP aggregates in the cell culture medium, which could
25 trigger stronger internalization by the B cells compared to well-dispersed polymer-coated
26 NPs.⁵⁰ It has recently been shown that NP-bound antigens can be efficiently taken up by
27 antigen-specific B lymphocytes, which then act as APCs to stimulate CD4 T cell responses.⁵¹
28 Taken together, polymer-coated GNPs loaded with antigen may selectively target only those B
29 lymphocytes recognizing their cognate antigen, thus enhancing selectivity of novel vaccine
30 strategies.
31
32
33
34
35
36
37
38
39
40
41
42
43
44
45
46
47
48

49 Cytotoxicity of GNPs, which depends on size, shape, dose, coating and surface
50 characteristics, is a major concern. Our results show that the formulations of GNPs used in this
51 study, including uncoated GNS and rod-shape GNPs, do not cause significant B cell
52 cytotoxicity after 24 h exposure *in vitro*. These results give us valuable information for the
53 further biomedical development of safe GNPs, particularly those that are foreseen to come in
54
55
56
57
58
59
60

1
2
3 direct contact with the immune system. In addition, gold nanomaterials have
4 immunomodulatory properties and are able to induce activation in immune cells.⁵² One of the
5 reasons is the insufficient GNP polymer surface coverage, which initiates binding and
6 deformation of proteins that can then act as immunostimulants.^{53,54} Our data provide evidence
7 that GNPs that are well-protected by polymers do not activate B lymphocytes, nor do they
8 interfere with the action of an immunostimulatory drug (R848).
9

10
11
12 Interestingly, we show that uncoated GNS, which aggregate in biological media, and rod-
13 shaped GNPs impaired IL-6 cytokine production in TLR7stimulated B lymphocytes. This
14 suggests that the particle shape controls interference with early, antigen-independent activation
15 events in B lymphocytes. However, further studies are needed to clarify possible mechanisms
16 behind this impairment.
17

18 CONCLUSION

19
20
21 The safety of NPs and their consequences on the immune system are of crucial importance.
22 Indeed, as stressed by FDA draft guidelines on nanomaterials for the industry, characterization
23 of the nanomaterial should be carefully assessed.⁵⁵ The defined physicochemical characteristics
24 of the NPs should be taken into consideration to cross-relate them for their stability in a
25 biological environment and to determine the exact mechanisms of cell type-specific biological
26 responses.⁷⁰ Therefore, to evaluate the adequacy of GNP use in clinical studies, the impact of
27 GNPs on the immune system (*e.g.*, immunogenicity and immunotoxicity) is an important aspect
28 that needs to be further investigated and specified. With our study, we have gained insight as to
29 the impact of GNPs on B lymphocytes and showed that the absence of polymer coating and
30 GNP shape are important factors that lead to different outcomes in GNP-B cell association and
31 B cell efficiency of the cytokine release, which should be considered for future development of
32 GNP for biomedical use.
33
34
35
36
37
38
39
40
41
42
43
44
45
46
47
48
49
50
51
52
53
54
55
56
57
58
59
60

METHODS

Chemicals and Reagents. All the chemicals were used without further purification. All chemicals and reagents purchased from Sigma-Aldrich (Switzerland) were used as received, unless otherwise stated.

GNP synthesis. Methoxy-polyethylene glycol thiol (mPEG-SH; 5 kDa) was purchased from Creative PEGWorks. Polyvinyl alcohol (PVA, Mowiol 3-85, 14 kDa) was purchased from Omy AG. All glassware was cleaned with *aqua regia* and extensively rinsed with water prior to use. Milli-Q grade water was used in all preparations.

Citrate-stabilized gold nanoparticles (GNPs) 15 nm in diameter, were synthesized as previously described by Turkevich et al.⁵⁶ Briefly, the aqueous solution of tetrachloroauric acid ($\text{HAuCl}_4 \times 3\text{H}_2\text{O}$; 500 mL, 0.5 mM) was heated to 100 °C and left to boil for 10 min, which was followed by rapid addition of 25 mL of 34 mM sodium citrate previously heated to 60 °C. Within 20 min the color of the solution changed to red, indicating the formation of GNPs. After cooling down to the room temperature, NPs were kept in the glass container, in the dark, and at a temperature of 4 °C.

Preparation of PEG-GNS. Aqueous solution of mPEG-SH (3.4 mg/mL, 2.5 mL), equivalent to 10 PEG nm⁻², were sonicated for 30 min and was subsequently mixed with 50 mL of citrate-coated GNS suspension. The mixture was left to react at room temperature for 24 h. To remove any excess polymer, the PEGylated GNS were centrifuged at 10000 ×g for 1h and redispersed in water.

Preparation of PEG/PVA-GNS. Separately, an aqueous solution containing 6 mg of polyvinyl alcohol (PVA) and 6 mg of mPEG-SH was prepared and sonicated for 20 min. Then, the polymer solution was added dropwise at room temperature under shaking to GNS suspension (20 mL). The mixture was left overnight under dark conditions. The final GNS-PEG/PVA

1
2
3 suspension was then centrifuged ($10000 \times g$, 1h) to remove excess polymer and re-dispersed in
4
5 water.
6

7
8 *Synthesis of GNRs.* GNRs were prepared by the seed-mediated growth method.⁵⁷ The Au
9
10 seeds were synthesized by mixing a hexadecyltrimethylammonium bromide (CTAB) solution
11
12 (0.1 M, 4.7 mL) with $\text{HAuCl}_4 \cdot 3\text{H}_2\text{O}$ (50 mM, 0.025 mL) at 28°C for 5 min. To this solution,
13
14 fresh sodium borohydride (NaBH_4) aqueous solution (10 mM, 0.3 mL) was added under
15
16 vigorous stirring for 2 min. The mixture immediately turned light brown indicating the
17
18 formation of seed particles. The seed dispersion was aged for 1 h at 28°C before using it.
19
20 Separately, a gold growth solution was prepared by adding $\text{HAuCl}_4 \cdot 3\text{H}_2\text{O}$ solution (50 mM,
21
22 2.23 mL) to CTAB (0.1 M, 200 mL) and mixed by inversion. Silver nitrate (AgNO_3) was then
23
24 added (10 mM, 2.6 mL), followed by HCl (1 M, 3.84 mL) and mixed again by inversion. Next,
25
26 L-ascorbic acid was added (0.1 M, 1.6mL) and the solution was mixed vigorously until the
27
28 solution turned colorless. Finally, the Au seeds (960 μL) were added to the growth solution and
29
30 followed by brief inversion mixing. The resulting suspension was left overnight at 28°C for the
31
32 GNRs formation. GNRs then underwent further manipulation in order to have a polymer
33
34 coating.
35
36
37
38
39

40
41 *Preparation of PEG-GNR by two steps method.* PEGylated GNRs were prepared as
42
43 previously described by Kinnear *et al.*²⁹ Briefly, the GNRs (10 mL, $[\text{Au}] = 0.15 \text{ mM}$) were
44
45 purified twice by centrifugation ($8000 \times g$ for 50 min) leading to a residual $[\text{CTAB}] = 0.1 \text{ mM}$.
46
47 Under shaking, a solution of mPEG-SH was added (10 mg/mL, 50.5 μL), equivalent to 10 PEG
48
49 nm^{-2} , and mixed over 24 hours. The partially PEGylated GNRs were then centrifuged at 8000
50
51 $\times g$ for 50 min and redispersed in ethanol (90% v/v ethanol, 9.5 mL). To this, an ethanolic
52
53 solution of mPEG-SH (1 mg/mL in 90% v/v ethanol, 505 μL) was added under shaking and
54
55 gently mixed over 24 hours. Finally, completely PEGylated GNRs were centrifuged three times
56
57
58
59
60

1
2
3 at 8000 × g for 50 min to remove unreacted PEG and displaced CTAB with redispersion in
4
5 water.
6
7
8
9

10 **GNP characterization.** *Transmission electron microscopy (TEM).* GNP diameter was
11 assessed through TEM, operating at 120 kV (FEI Technai Spirit microscope, USA) and
12 equipped with Veleta CDD camera (Olympus, Japan). In order to avoid drying-related artifacts
13 of drop-casting, Citrate-GNS and PEG-GNRs TEM samples were prepared as previously
14 described.⁵⁸ Briefly, samples were suspended to 1:1 ratio in the corresponding concentration of
15 bovine serum albumin (BSA, Sigma-Aldrich, USA) solution and left at 4 °C overnight.
16 Polymer-coated GNS samples were prepared without BSA incubation, in order to obtain more
17 dense images of these type of NPs. A total of 5 µl of BSA-GNP (citrate-GNS, PEG-GNR) or
18 GNP sample in H₂O alone (PEG-GNS, PEG/PVA-GNS) was drop-casted on mesh copper grids
19 at a final GNP concentration 20 µg/mL and left to dry at room temperature. GNP size was
20 subsequently calculated using ImageJ software at the following NP count: Citrate-GNS: n=132;
21 PEG-GNS: n=103, PEG/PVA-GNS: n=149, PEG-GNR: n=220. Endotoxin levels of GNPs
22 were determined by Pierce LAL Chromogenic Endotoxin Quantitation Kit (ThermoFisher,
23 Switzerland), following the manufacturer's guidelines (Figure S9).
24
25
26
27
28
29
30
31
32
33
34
35
36
37
38
39
40
41

42 *UV-Vis.* UV-Vis spectra of GNPs was obtained using Jasco V-670 spectrophotometer. The
43 colloidal stability was tested by incubation of GNPs in H₂O, 10mM PBS and culture medium
44 (RPMI 1640 (Roswell Park Memorial Institute) with 10% human plasma, 1% PenStrep and 1%
45 L-Glutamine) for 24 h at 37 °C, 5% CO₂. All GNPs were diluted to concentration 0.01 mg/ml
46 in each solution.
47
48
49
50
51
52
53

54 *Dynamic depolarized light scattering (DDLS).* Citrate-GNS, PEG-GNS, PEG/PVA-GNS (all
55 at 5 µg/mL) and PEG-GNR (20 µg/mL) were incubated in water or culture medium (RPMI with
56 10% human plasma, 1 % PenStrep and 1% L-Glutamine), at 37 °C for 24 h. Then, dynamic
57
58
59
60

1
2
3 depolarized light scattering (DDLS) measurements were performed at constant temperature (21
4 °C) at scattering angle of 30°, using a commercial goniometer instrument (3D LS Spectrometer,
5 LS Instruments AG, Switzerland). To estimate the number-averaged hydrodynamic radii, the
6 DDLS spectra were analyzed by the approach presented elsewhere.⁵⁹
7
8
9

10
11
12 *ζ-potential.* GNP charge was acquired with phase amplitude light scattering analyzer (PALS)
13 (Brookhaven ZetaPALS). GNPs were measured at 0.05 mg/ml, at RT in H₂O (pH 7), PBS (pH
14 7) and culture media (pH 7), where PBS and media were pre-diluted in H₂O to 1:10.
15 Measurements for each sample were obtained using the Smoluchowski model⁶⁰ with 10 cycles
16 of electrophoretic mobility (EPM) and 10 repetitions to gain mean and standard deviation data.
17 All incubations of GNP in the cell-free biological media were solely performed for GNP
18 characterization purposes.
19
20
21
22
23
24
25
26
27
28
29

30
31 **Immune cell cultures.** *Human B lymphocytes.* Buffy coats from healthy donors
32 (BlutZentrum, Bern, Switzerland) were separated by gradient density (Lymphoprep™,
33 Stemcell Technologies, Canada) followed by specific B lymphocyte magnetic bead isolation
34 using anti-CD20 MicroBeads (Miltenyi Biotec, Germany). Fc receptor blocking reagent
35 (Miltenyi Biotec) was added according to the manufacturer's instructions. A purity of > 96%
36 CD20⁺ cells was obtained throughout the experiments (Figure S5). B lymphocytes were
37 cultured in 6-well plates (0.25x10⁶ cells/ml) at 37° C, 5% CO₂ in RPMI 1640, supplemented
38 with 10% autologous human plasma from each donor, 1% PenStrep (ThermoFisher Scientific,
39 USA, #15140122) and 1% L-Glutamine (ThermoFisher, Scientific, USA, #25030081). The
40 seeding concentration was chosen based on the median B lymphocyte number typically found
41 in healthy human peripheral blood.⁶¹
42
43
44
45
46
47
48
49
50
51
52
53
54

55
56 *Monocyte sub-culture.* Monocytes were isolated from buffy coats with anti-CD14
57 MicroBeads (Miltenyi Biotec) and cultured in 6-well plates (10⁶ cells/ml).⁶² Fc receptor
58
59
60

1
2
3 blocking reagent (Miltenyi Biotec) was added in the purification protocol. In order to
4
5 differentiate monocytes to macrophages (monocyte-derived macrophages, MDM) or dendritic
6
7 cells (monocyte-derived dendritic cells, MDDC), 10 ng/ml macrophage colony-stimulating
8
9 factor (M-CSF) or 10 ng/ml granulocyte-macrophage colony-stimulating factor (GM-CSF) and
10
11 10 ng/ml IL-4 were added into the culture, respectively, and incubated for 6 days at 37° C,
12
13 5%CO₂. All cell types were cultured at 37° C, 5% CO₂ in RPMI 1640, supplemented with 10%
14
15 autologous human plasma from each donor, 1% PenStrep (ThermoFisher Scientific, USA,
16
17 #15140122) and 1% L-Glutamine (ThermoFisher, Scientific, USA, #25030081).
18
19
20
21
22

23
24 **Exposure to GNPs and stimulants.** *B lymphocytes.* Cells were exposed to all GNS directly
25
26 after purification for 24 h, at concentrations from 5-20 µg/ml and to PEG-GNRs at 20 µg/ml.
27

28
29 *MDMs/MDDCs.* Cells were exposed to all GNS on day 6 of culture at 20 µg/ml for 24 h.
30
31 R848 (Enzo, USA) at 2 µg/ml was used for B lymphocyte/MDMs/MDDMs and LPS control at
32
33 100 ng/ml (Sigma-Aldrich, Switzerland) was used for MDM/MDDCs stimulation. The working
34
35 concentrations of these immunostimulants was selected in order to induce robust activation in
36
37 all donor samples.
38
39

40
41
42 **GNP-cell association assessment.** *Light microscopy.* Phase contrast images were captured
43
44 at a magnification ×40, using an inverted light microscope (Motic AE2000, Germany) after 24
45
46 h NP exposure (Figure S1).
47

48
49 *Enhanced dark-field optical microscopy with high-resolution hyperspectral imaging.* Cells
50
51 exposed to GNPs were fixed with 4% paraformaldehyde (PFA), permeabilized with 0.01%
52
53 TritonX-100 (Sigma-Aldrich, Switzerland) in PBS and stained with Rhodamine-Phalloidin,
54
55 diluted 1:40 in PBS and 4',6-diamidino-2-phenylindole (DAPI) using dilution 1:100 in PBS.
56
57 Samples were imaged with high signal to noise ratio dark field hyperspectral imaging that uses
58
59
60

1
2
3 oblique angle lighting (CytoViva, Alburn, Alabama, US). The system is coupled with an
4
5 Olympus BX-51 microscope outfitted with a fluorescence light source (X-Cite series 120),
6
7 halogen light source (Dolan-Jenner DC-950), UPL Fluorite 100× objective, and SPECIM V10E
8
9 imaging spectrograph with a PCO pixelfly detector (Kelhelm, Germany). All data acquisition
10
11 was performed using the same exposure time and magnification (100x oil immersion). Images
12
13 from both dark field and fluorescent imaging were recorded using a 3D Exi blue camera
14
15 (QImaging, Surry, Canada) and ENVI 4.8 software. Images obtained from both sources were
16
17 overlaid using Image J software. Hyperspectral images were recorded using the same system
18
19 and software but in spectral mode, using above mentioned detector. Due to the strong scattering
20
21 of light, gold nanoparticles appear as the brightest signal on the image. Linear enhancement
22
23 was used to obtain the best contrast of the object against the image background. This type of
24
25 enhancement shows the full intensity range, from lowest to highest, without clipping.
26
27
28
29
30
31
32

33 *ICP-MS. Chemicals:* Acids (HNO₃, HCl) were of PlasmaPure grade from SCP Science
34
35 (Courtaboeuf, France). Ultrapure de-ionized water was provided by an Integral 3 Advantage
36
37 A10 purification system (Merck-Millipore, Schaffhausen, Switzerland). The ICP-MS certified
38
39 tuning solution consisted of 1 µg/L each of Li, Mg, Y, Ce, Tl and Co in a matrix of 2% HNO₃
40
41 was from SCP Science (cat n°701-021-194 5185-5959, batch n°S171122014). The gold
42
43 certified standard solution (1000 ppm in 5% HCl) was purchased from Sigma-Aldrich (cat
44
45 n°38168-100ML, batch n°BCBT4405).
46
47
48

49 *Sample preparation:* B lymphocytes and MDMs were cultured and exposed to GNPs as
50
51 described above. After 24 h, cells of 1-3 plates were pooled (cells in 18-54 ml), washed two
52
53 times in 1x PBS (500 × g, 4 °C, 5 min) and counted (total cell number of the sample). After
54
55 final centrifugation, supernatant was discarded and cell pellets were stored at -20 °C until
56
57 further analysis. Cell pellets were re-suspended in 4.5 mL ultrapure Milli-Q water, with addition
58
59
60

1
2
3 of 0.5 mL of concentrated Aqua Regia (HNO₃:HCl, 1:3), and digested by heating block for 1
4
5 hour at 80°C (EasyDigest, Analab, France). Then, digested cell pellets were diluted in 10%(v/v)
6
7 aqueous Aqua Regia (10% AR) to be within the calibration range of the ICP-MS method. Final
8
9 quantification of GNP-cell association was calculated as ng/10⁶ cells by dividing measured
10
11 GNP mass per total cell number of each sample (cell count prior obtaining the cell pellet) and
12
13 multiplication by 10⁶.
14
15

16
17 *Instrumentation:* The Agilent 7700x ICP-MS system (Agilent Technologies, Basel,
18
19 Switzerland) was equipped with a Micromist nebulizer and a Scott type spray chamber. The
20
21 ICP-MS parameters were tuned with a certified solution to obtain the best sensitivity, resolution
22
23 and the lower RSD on ⁷Li, ⁸⁹Y and ²⁰⁵Tl, and also the lower oxide (156/140, CeO/Ce) and
24
25 doubly charged (70/140, Ce²⁺/Ce) ratios. The ICP-MS parameters were optimized for the three
26
27 collision cell modes (Table S1).
28
29

30
31 *ICP-MS method:* Gold (¹⁹⁷Au) was quantified (n=3) by ICP-MS with and without the use of
32
33 a collision cell (CC), respectively termed [He] or [HEHe] and [No gas] mode. The two collision
34
35 cell modes, [He] and [HEHe], with Helium gas at two flow rates: 4.3 mL/min and 10 mL/min,
36
37 respectively, allow removing or reducing the potential spectral interferences. The ICP-MS
38
39 calibration curve consisted of one blank (10% AR) and eight ¹⁹⁷Au concentration levels (0.1,
40
41 0.5, 1, 5, 10, 15, 20, 25 ppb in 10% AR). The linear regression correlation coefficients (R) were
42
43 equal to 0.9997, 0.9995 and 0.9995 for ¹⁹⁷Au measured in [No Gas], [He] and [HEHe] modes,
44
45 respectively (Figure S2), which was in agreement with the FDA guidelines (R ≥ 0.998).⁶³
46
47 Evaluation of the ICP-MS method accuracy and precision was also evaluated. The results fulfill
48
49 the precision (RSD ≤ 15%) and accuracy (100% ± 15%) criteria.⁴³
50
51
52

53
54 **Flow cytometry – Cell viability and immune cell status.** Cells were stained for 15 min at
55
56 room temperature with Zombie NIR™ Fixable Viability Kit (BioLegend, USA) and washed
57
58 with FACS buffer (1% BSA, 0.5% sodium azide (Sigma-Aldrich, Switzerland) in PBS). Cells
59
60

1
2
3 were then stained for 30 min with the following antibodies at 1:100 (unless stated otherwise).
4
5 *B cells*: anti-human CD20-FITC (B cell-specific marker, BD Biosciences, USA), anti-human
6 CD69-Pacific Blue™ (BioLegend, USA), CD86-PE-Cy5 (BioLegend, USA) and HLA-DR-
7 PE-CF594 (at 1:300, BD Biosciences, USA); *MDMs*: CD14-FITC (monocyte/macrophage-
8 specific marker, BioLegend, USA), CD69-PacificBlue (BioLegend, USA), CD86-PE-Cy5
9 (BioLegend, USA), HLA-DR-PE-CF594 (at 1:300, BD Biosciences, USA); MDDCs: CD1c-
10 PacificBlue (dendritic cell-specific marker, BioLegend, USA), CD80-FITC, CD86-PE-Cy5
11 (BioLegend, USA), HLA-DR-PE-CF594 (at 1:300, BD Biosciences, USA). Cells were then
12 washed and re-suspended in 0.5 ml FACS buffer for flow cytometer analysis (BD LSR Fortessa,
13 Switzerland). Three independent experiments were performed for each cell type and each
14 sample was set up to capture up to 30,000 events. Gating strategies for all cell types are shown
15 and explained in the supplementary information (Figure S5). All flow cytometry data were
16 analyzed with FlowJo software (Version 10, Tree Star, USA).
17
18
19
20
21
22
23
24
25
26
27
28
29
30
31
32

33 **Pro-inflammatory response.** After 24 h exposure of immune cells to GNPs, culture
34 supernatants were collected and measured for concentrations of interleukin (IL)-6, IL-1 β and
35 tumor necrosis factor(TNF)- α by ELISA. The assay was performed according to the
36 manufacturer's instructions (Human IL-6 DuoSet ELISA, Human IL-1 β /IL-1F2 DuoSet ELISA
37 and Human TNF- α DuoSet ELISA, all from R&D, USA). The experiment for each analyte was
38 conducted three times in duplicates (n=3).
39
40
41
42
43
44
45
46

47 To ensure that GNPs did not interfere with the spectrophotometric analysis, an interference
48 test were performed for IL-6 ELISA kit: GNPs (20 μ g/ml) alone were incubated in complete
49 culture media for 24 h at 37 °C, 5% CO₂. Prior to the ELISA being conducted, GNP samples
50 were incubated with a IL-6 standard (0-600 pg/ml) for 1 h at RT. Optical density for all the
51 ELISA samples was measured at 450/570 nm, using a microplate reader (Benchmark
52
53
54
55
56
57
58
59
60

1
2
3 Microplate reader, BioRad, Cressier, Switzerland). The test experiments were performed once
4
5 in triplicate (Figure S8).
6

7 **Data and Statistical Analysis.** Results are presented as a mean of three separate experiments
8
9 (three different donors (n=3)) \pm standard deviation (SD). Data were considered normally
10
11 distributed and thus were evaluated using a non-parametric two-way analysis of variance
12
13 (ANOVA) or one-way ANOVA. Subsequent analysis occurred in terms of a Tukey's multiple
14
15 comparison *post-hoc* test (GraphPad Prism 7 software, USA). Data was considered significant
16
17 when $*p<0.05$, $**p<0.01$ and $***p<0.001$.
18
19
20
21
22
23

24 ASSOCIATED CONTENT

25 26 27 **Supporting Information**

28
29
30
31 The Supporting Information is available free of charge on the <http://pubs.acs.org>

32
33
34 SEM method (Abstract Graphic), light microscopy images of APCs, details about
35
36 optimization of the ICP-MS method, additional DF-HSI image, GNP-cell association and
37
38 FSC/SSC signal, cell purity and gating strategy, MDM and MDDC activation, MDM and
39
40 MDDC pro-inflammatory response, GNP interference test.
41
42
43

44 AUTHOR INFORMATION

45 46 47 **Corresponding Authors**

48
49
50 *Martin J.D. Clift, e-mail: m.j.d.clift@swansea.ac.uk.

51
52
53 *Carole Bourquin, e-mail: carole.bourquin@unige.ch.

54 55 56 **Present Addresses**

57
58
59 †Empa, 9014 St. Gallen, Switzerland
60

1
2
3 §Nano4Environment Unit, Water Quality Group, INL - International Iberian Nanotechnology
4
5 Laboratory, 4715-330 Braga, Portugal
6
7

8 **Author Contributions**

9

10
11 SH participated in the design of the study, performed UV-Vis and TEM measurements, all
12 biological experimentation and analyzed the data. AM carried out DF-HSI measurements.
13
14 DDLS was performed and analyzed by AM and LR-L. Synthesis of nanoparticles was
15
16 conducted by LA-H. IM contributed as an advisor of the flow cytometry experiments. AP-F
17
18 and BR-R participated in supervision of the experimental work and gave expert advice. CB and
19
20 MJDC designed the project and supervised the experimental work. The manuscript was written
21
22 by SH, CB and MJDC and commented by all authors.
23
24
25
26

27
28 *These authors contributed equally.
29
30
31
32
33

34 **ACKNOWLEDGMENTS**

35

36
37
38 The authors acknowledge the support by the Swiss National Science Foundation (SNSF)
39 through the National Centre of Competence in Research “Bio-Inspired Nanomaterials” and
40 projects no. 156871, 156372 and 182317, the Adolphe Merkle foundation (Fribourg,
41
42 Switzerland), and the MZ 2.0 mass spectrometry core facility (University of Geneva) for the
43
44 ICP-MS method development and sample measurements.
45
46
47
48
49
50
51
52
53
54
55
56
57
58
59
60

REFERENCES

- (1) Lebien, T. W.; Tedder, T. F. ASH 50th Anniversary Review B Lymphocytes : How They Develop and Function. *Am. Soc. Hematol.* **2008**, *112*, 1570–1580.
- (2) Pardi, N.; Hogan, M. J.; Naradikian, M. S.; Parkhouse, K.; Cain, D. W.; Jones, L.; Moody, M. A.; Verkerke, H. P.; Myles, A.; Willis, E.; LaBranche, C. C.; Montefiori, D. C.; Lobby, J. L.; Saunders, K. O.; Liao, H.-X.; Korber, B. T.; Sutherland, L. L.; Scarce, R. M.; Hraber, P. T.; et al. Nucleoside-Modified mRNA Vaccines Induce Potent T Follicular Helper and Germinal Center B Cell Responses. *J. Exp. Med.* **2018**, *215*, 1571–1588.
- (3) Fenton, O. S.; Kauffman, K. J.; Kaczmarek, J. C.; McClellan, R. L.; Jhunjunwala, S.; Tibbitt, M. W.; Zeng, M. D.; Appel, E. A.; Dorkin, J. R.; Mir, F. F.; Yang, J. H.; Oberli, M. A.; Heartlein, M. W.; DeRosa, F.; Langer, R.; Anderson, D. G. Synthesis and Biological Evaluation of Ionizable Lipid Materials for the *In Vivo* Delivery of Messenger RNA to B Lymphocytes. *Adv. Mater.* **2017**, *29*, 1–7.
- (4) Shen, X.; Pasha, M. A.; Hidde, K.; Khan, A.; Liang, M.; Guan, W.; Ding, Y.; Haczku, A.; Yang, Q. Group 2 Innate Lymphoid Cells Promote Airway Hyperresponsiveness through Production of VEGFA. *J. Allergy Clin. Immunol.* **2018**, *141*, 1929-1931.e4.
- (5) Hua, Z.; Hou, B. TLR Signaling in B-Cell Development and Activation. *Cell. Mol. Immunol.* **2013**, *10*, 103–106.
- (6) Boraschi, D.; Italiani, P.; Palomba, R.; Decuzzi, P.; Duschl, A.; Fadeel, B.; Moghimi, S. M. Nanoparticles and Innate Immunity: New Perspectives on Host Defence. *Semin. Immunol.* **2017**, *34*, 33–51.
- (7) Kojima, S.; Negishi, Y.; Tsukimoto, M.; Takenouchi, T.; Kitani, H.; Takeda, K. Purinergic Signaling *via* P2X₇ Receptor Mediates IL-1 β Production in Kupffer Cells Exposed to Silica Nanoparticle. *Toxicology* **2014**, *321*, 13–20.

- 1
2
3 (8) Turabekova, M.; Rasulev, B.; Theodore, M.; Jackman, J.; Leszczynska, D.; Leszczynski, J.
4
5 Immunotoxicity of Nanoparticles: A Computational Study Suggests That CNTs and C₆₀
6
7 Fullerenes Might Be Recognized as Pathogens by Toll-like Receptors. *Nanoscale* **2014**, *6*, 3488–
8
9 3495.
10
11
12 (9) Xi, C.; Zhou, J.; Du, S.; Peng, S. Autophagy Upregulation Promotes Macrophages to Escape
13
14 Mesoporous Silica Nanoparticle (MSN)-Induced NF- κ B-Dependent Inflammation. *Inflamm.*
15
16 *Res* **2016**, *65*, 325–341.
17
18
19 (10) Debotton, N.; Dahan, A. Applications of Polymers as Pharmaceutical Excipients in Solid Oral
20
21 Dosage Forms. *Med. Res. Rev.* **2017**, *37*, 52–97.
22
23
24 (11) European Food Safety Authority (EFSA). Scientific Opinion on the Safety of Polyvinyl Alcohol-
25
26 Polyethylene Glycol-Graft-Co-Polymer as a Food Additive. *EFSA J.* **2013**, *11*, 3303.
27
28
29 (12) Lubich, C.; Allacher, P.; de la Rosa, M.; Bauer, A.; Prenninger, T.; Horling, F. M.; Siekmann,
30
31 J.; Oldenburg, J.; Scheiflinger, F.; Reipert, B. M. The Mystery of Antibodies Against
32
33 Polyethylene Glycol (PEG) - What Do We Know? *Pharm. Res.* **2016**, *33*, 2239–2249.
34
35
36 (13) Dykman, L.; Khlebtsov, N. Gold Nanoparticles in Biomedical Applications: Recent Advances
37
38 and Perspectives. *Chem. Soc. Rev.* **2012**, *41*, 2256–2282.
39
40
41 (14) Climent, N.; García, I.; Marradi, M.; Chiodo, F.; Miralles, L.; José Maleno, M.; María Gatell, J.;
42
43 García, F.; Penadés, S.; Plana, M. Loading Dendritic Cells with Gold Nanoparticles (GNPs)
44
45 Bearing HIV- Peptides and Mannosides Enhance HIV-Specific T Cell Responses. *Nanomedicine*
46
47 **2018**, *14*, 339–351.
48
49
50 (15) Assis, N. R. G.; Caires, A. J.; Figueiredo, B. C.; Morais, S. B.; Mambelli, F. S.; Marinho, F. V.;
51
52 Ladeira, L. O.; Oliveira, S. C. The Use of Gold Nanorods as a New Vaccine Platform against
53
54 Schistosomiasis. *J. Control. Release* **2018**, *275*, 40–52.
55
56
57 (16) Rodriguez-Lorenzo, L.; Fytianos, K.; Blank, F.; Von Garnier, C.; Rothen-Rutishauser, B.; Petri-
58
59 Fink, A. Fluorescence-Encoded Gold Nanoparticles: Library Design and Modulation of Cellular
60

- 1
2
3 Uptake into Dendritic Cells. *Small* **2014**, *10*, 1341–1350.
4
5
6 (17) Kinnear, C.; Rodriguez-Lorenzo, L.; Clift, M. J. D.; Goris, B.; Bals, S.; Rothen-Rutishauser, B.;
7
8 Petri-Fink, A. Decoupling the Shape Parameter to Assess Gold Nanorod Uptake by Mammalian
9
10 Cells. *Nanoscale* **2016**, *8*, 16416–16426.
11
12
13 (18) Ho, L. W. C.; Yung, W.-Y.; Sy, K. H. S.; Li, H. Y.; Choi, C. K. K.; Leung, K. C.-F.; Lee, T. W.
14
15 Y.; Choi, C. H. J. Effect of Alkylation on the Cellular Uptake of Polyethylene Glycol-Coated
16
17 Gold Nanoparticles. *ACS Nano* **2017**, *11*, 6085–6101.
18
19
20 (19) Ji, Z.; Jin, X.; George, S.; Xia, T.; Meng, H.; Wang, X.; Suarez, E.; Zhang, H.; Hoek, E. M. V.;
21
22 Godwin, H.; Nel, A. E.; Zink, J. I. Dispersion and Stability Optimization of TiO₂ Nanoparticles
23
24 in Cell Culture Media. *Environ. Sci. Technol.* **2010**, *44*, 7309–7314.
25
26
27 (20) Yang, S.-A.; Choi, S.; Jeon, S. M.; Yu, J. Silica Nanoparticle Stability in Biological Media
28
29 Revisited. *Sci. Rep.* **2018**, *8*, 185.
30
31
32 (21) Jiang, W.; Hibbert, D. B.; Moran, G.; Herrmann, J.; Jämting, Å. K.; Coleman, V. A.
33
34 Characterisation of Gold Agglomerates: Size Distribution, Shape and Optical Properties. *RSC*
35
36 *Adv.* **2013**, *3*, 7367.
37
38
39 (22) Dobrovolskaia, M. A.; Patri, A. K.; Zheng, J.; Clogston, J. D.; Ayub, N.; Aggarwal, P.; Neun, B.
40
41 W.; Hall, J. B.; McNeil, S. E. Interaction of Colloidal Gold Nanoparticles with Human Blood:
42
43 Effects on Particle Size and Analysis of Plasma Protein Binding Profiles. *Nanomedicine*
44
45 *Nanotechnology, Biol. Med.* **2009**, *5*, 106–117.
46
47
48 (23) Piella, J.; Bastús, N. G.; Puentes, V. Size-Dependent Protein–Nanoparticle Interactions in Citrate-
49
50 Stabilized Gold Nanoparticles: The Emergence of the Protein Corona. *Bioconjug. Chem.* **2017**,
51
52 *28*, 88–97.
53
54
55 (24) Liu, Z.; Zhan, X.; Xu, X.; Wu, Y.; Gu, Z. Static Magnetic Field Dictates Protein Corona
56
57 Formation on the Surface of Glutamine-Modified Superparamagnetic Iron Oxide Nanoparticles.
58
59 *Part. Part. Syst. Charact.* **2018**, *35*, 1700418.
60

- 1
2
3 (25) Manson, J.; Kumar, D.; Meenan, B. J.; Dixon, D. Polyethylene Glycol Functionalized Gold
4 Nanoparticles: The Influence of Capping Density on Stability in Various Media. *Gold Bull.* **2011**,
5 *44*, 99–105.
6
7
8
9
10 (26) Rahme, K.; Chen, L.; Hobbs, R. G.; Morris, M. A.; O'Driscoll, C.; Holmes, J. D. PEGylated
11 Gold Nanoparticles: Polymer Quantification as a Function of PEG Lengths and Nanoparticle
12 Dimensions. *RSC Adv.* **2013**, *3*, 6085–6094.
13
14
15
16
17 (27) Uz, M.; Bulmus, V.; Alsoy Altinkaya, S. Effect of PEG Grafting Density and Hydrodynamic
18 Volume on Gold Nanoparticle–Cell Interactions: An Investigation on Cell Cycle, Apoptosis, and
19 DNA Damage. *Langmuir* **2016**, *32*, 5997–6009.
20
21
22
23
24 (28) Allen, J. M.; Xu, J.; Blahove, M.; Canonico-May, S. A.; Santaloci, T. J.; Braselton, M. E.; Stone,
25 J. W. Synthesis of Less Toxic Gold Nanorods by Using Dodecylethyldimethylammonium
26 Bromide as an Alternative Growth-Directing Surfactant. *J. Colloid Interface Sci.* **2017**, *505*,
27 1172–1176.
28
29
30
31
32
33 (29) Kinnear, C.; Dietsch, H.; Clift, M. J. D.; Endes, C.; Rothen-Rutishauser, B.; Petri-Fink, A. Gold
34 Nanorods: Controlling Their Surface Chemistry and Complete Detoxification by a Two-Step
35 Place Exchange. *Angew. Chemie Int. Ed.* **2013**, *52*, 1934–1938.
36
37
38
39
40 (30) He, C.; Hu, Y.; Yin, L.; Tang, C.; Yin, C. Effects of Particle Size and Surface Charge on Cellular
41 Uptake and Biodistribution of Polymeric Nanoparticles. *Biomaterials* **2010**, *31*, 3657–3666.
42
43
44
45 (31) Yue, Z.-G.; Wei, W.; Lv, P.-P.; Yue, H.; Wang, L.-Y.; Su, Z.-G.; Ma, G.-H. Surface Charge
46 Affects Cellular Uptake and Intracellular Trafficking of Chitosan-Based Nanoparticles.
47 *Biomacromolecules* **2011**, *12*, 2440–2446.
48
49
50
51 (32) Blundell, E. L. C. J.; Healey, M. J.; Holton, E.; Sivakumaran, M.; Manstana, S.; Platt, M.
52
53
54
55
56
57
58
59
60
60

- 1
2
3 (33) Gräfe, C.; Weidner, A.; Lühe, M. V. D.; Bergemann, C.; Schacher, F. H.; Clement, J. H.; Dutz,
4 S. Intentional Formation of a Protein Corona on Nanoparticles: Serum Concentration Affects
5 Protein Corona Mass, Surface Charge, and Nanoparticle–Cell Interaction. *Int. J. Biochem. Cell*
6 *Biol.* **2016**, *75*, 196–202.
7
8
9
10
11
12 (34) Mottas, I.; Milosevic, A.; Petri-Fink, A.; Rothen-Rutishauser, B.; Bourquin, C. A Rapid
13 Screening Method to Evaluate the Impact of Nanoparticles on Macrophages. *Nanoscale* **2017**, *9*,
14 2492–2504.
15
16
17
18
19 (35) Villiers, C.; Freitas, H.; Couderc, R.; Villiers, M.-B.; Marche, P. Analysis of the Toxicity of Gold
20 Nano Particles on the Immune System: Effect on Dendritic Cell Functions. *J. Nanopart. Res.*
21 **2010**, *12*, 55–60.
22
23
24
25
26 (36) Fytianos, K.; Rodriguez-Lorenzo, L.; Clift, M. J. D.; Blank, F.; Vanhecke, D.; von Garnier, C.;
27 Petri-Fink, A.; Rothen-Rutishauser, B. Uptake Efficiency of Surface Modified Gold
28 Nanoparticles Does Not Correlate with Functional Changes and Cytokine Secretion in Human
29 Dendritic Cells *In Vitro*. *Nanomedicine* **2015**, *11*, 633–644.
30
31
32
33
34
35 (37) Morbach, H.; Eichhorn, E. M.; Liese, J. G.; Girschick, H. J. Reference Values for B Cell
36 Subpopulations from Infancy to Adulthood. *Clin. Exp. Immunol.* **2010**, *162*, 271–279.
37
38
39
40 (38) Bishop, G. A.; Ramirez, L. M.; Baccam, M.; Busch, L. K.; Pederson, L. K.; Tomai, M. A. The
41 Immune Response Modifier Resiquimod Mimics CD40-Induced B Cell Activation. *Cell*
42 *Immunol.* **2001**, *208*, 9–17.
43
44
45
46 (39) Douagi, I.; Gujer, C.; Sundling, C.; Adams, W. C.; Smed-Sörensen, A.; Seder, R. A.; Karlsson
47 Hedestam, G. B.; Loré, K. Human B Cell Responses to TLR Ligands Are Differentially
48 Modulated by Myeloid and Plasmacytoid Dendritic Cells. *J Immunol.* **2009**, *182*, 1991–2001.
49
50
51
52 (40) Souwer, Y.; Griekspoor, A.; Jorritsma, T.; de Wit, J.; Janssen, H.; Neefjes, J.; van Ham, S. M. B
53 Cell Receptor-Mediated Internalization of *Salmonella*: A Novel Pathway for Autonomous B Cell
54 Activation and Antibody Production. *J. Immunol.* **2009**, *182*, 7473–7481.
55
56
57
58
59
60

- 1
2
3 (41) Gustafson, H. H.; Holt-Casper, D.; Grainger, D. W.; Ghandehari, H. Nanoparticle Uptake: The
4 Phagocyte Problem. *Nano Today* **2015**, *10*, 487–510.
5
6
7
8 (42) Zucker, R. M. D. of T. nanoparticles in cells by flow cytometry; Massaro, E. J.; Sanders, K. M.;
9 Degn, L. L.; Boyes, W. K. Detection of TiO₂ Nanoparticles in Cells by Flow Cytometry. *Cytom.*
10 *A. A* **2010**, *77A*, 677–685.
11
12
13
14
15 (43) Levine, K. E.; Tudan, C.; Grohse, P. M.; Weber, F. X.; Levine, M. A.; Kim, Y.-S. J. Aspects of
16 Bioanalytical Method Validation for the Quantitative Determination of Trace Elements.
17 *Bioanalysis* **2011**, *3*, 1699–1712.
18
19
20
21
22 (44) Sharma, M.; Salisbury, R. L.; Maurer, E. I.; Hussain, S. M.; Sulentic, C. E. W. Gold
23 Nanoparticles Induce Transcriptional Activity of NF-KB in a B-Lymphocyte Cell Line.
24 *Nanoscale* **2013**, *5*, 3747–3756.
25
26
27
28
29 (45) Lee, C.-H.; Syu, S.-H.; Chen, Y.-S.; Hussain, S. M.; Aleksandrovich Onischuk, A.; Chen, W. L.;
30 Steven Huang, G. Gold Nanoparticles Regulate the Blimp1/Pax5 Pathway and Enhance
31 Antibody Secretion in B-Cells. *Nanotechnology* **2014**, *25*, 125103.
32
33
34
35
36 (46) Dorner, M.; Brandt, S.; Tinguely, M.; Zucol, F.; Bourquin, J.-P.; Zauner, L.; Berger, C.;
37 Bernasconi, M.; Speck, R. F.; Nadal, D. Plasma Cell Toll-like Receptor (TLR) Expression
38 Differs from That of B Cells, and Plasma Cell TLR Triggering Enhances Immunoglobulin
39 Production Introduction. *Immunology* **2009**, *128*, 573–579.
40
41
42
43
44
45 (47) Nicolete, R.; dos Santos, D. F.; Faccioli, L. H. The Uptake of PLGA Micro or Nanoparticles by
46 Macrophages Provokes Distinct *In Vitro* Inflammatory Response. *Int. Immunopharmacol.* **2011**,
47 *11*, 1557–1563.
48
49
50
51
52 (48) Silva, A. L.; Peres, C.; Coniot, J.; Matos, A. I.; Moura, L.; Carreira, B.; Sainz, V.; Scomparin,
53 A.; Satchi-Fainaro, R.; Pr eat, V.; Florindo, H. F. Nanoparticle Impact on Innate Immune Cell
54 Pattern-Recognition Receptors and Inflammasomes Activation. *Semin. Immunol.* **2017**, *34*, 3–
55
56
57
58
59
60 24.

- 1
2
3 (49) Zhu, Q.; Zhang, M.; Shi, M.; Liu, Y.; Zhao, Q.; Wang, W.; Zhang, G.; Yang, L.; Zhi, J.; Zhang,
4 L.; Hu, G.; Chen, P.; Yang, Y.; Dai, W.; Liu, T.; He, Y.; Feng, G.; Zhao, G. Human B Cells Have
5 an Active Phagocytic Capability and Undergo Immune Activation upon Phagocytosis of
6 Mycobacterium Tuberculosis. *Immunobiology* **2016**, *221*, 558–567.
7
8
9
10
11
12 (50) Lichtenstein, D.; Meyer, T.; Böhmert, L.; Juling, S.; Fahrenson, C.; Selve, S.; Thünemann, A.;
13 Meijer, J.; Estrela-Lopis, I.; Braeuning, A.; Lampen, A. Dosimetric Quantification of Coating-
14 Related Uptake of Silver Nanoparticles. *Langmuir* **2017**, *33*, 13087–13097.
15
16
17
18
19 (51) Hong, S.; Zhang, Z.; Liu, H.; Tian, M.; Zhu, X.; Zhang, Z.; Wang, W.; Zhou, X.; Zhang, F.; Ge,
20 Q.; Zhu, B.; Tang, H.; Hua, Z.; Hou, B. B Cells Are the Dominant Antigen-Presenting Cells That
21 Activate Naive CD4+ T Cells upon Immunization with a Virus-Derived Nanoparticle Antigen.
22 *Immunity* **2018**, *49*, 1–14.
23
24
25
26
27
28
29 (52) Le Gú, X.; Palomares, F.; Torres, M. J.; Blanca, M.; Fernandez, T. D.; Mayorga, C. Nanoparticle
30 Size Influences the Proliferative Responses of Lymphocyte Subpopulations. *RSC Adv.* **2015**, *5*,
31 85305–85309.
32
33
34
35
36 (53) Saptarshi, S. R.; Duschl, A.; Lopata, A. L. Interaction of Nanoparticles with Proteins: Relation
37 to Bio-Reactivity of the Nanoparticle. *J. Nanobiotechnology* **2013**, *11*, 26.
38
39
40
41 (54) Mortimer, G. M.; Butcher, N. J.; Musumeci, A. W.; Deng, Z. J.; Martin, D. J.; Minchin, R. F.
42 Cryptic Epitopes of Albumin Determine Mononuclear Phagocyte System Clearance of
43 Nanomaterials. *ACS Nano* **2014**, *8*, 3357–3366.
44
45
46
47
48 (55) Food and Drug Administration (FDA). Drug Products, Including Biological Products, that Contain
49 Nanomaterials - Guidance for Industry
50 [https://www.fda.gov/downloads/Drugs/GuidanceComplianceRegulatoryInformation/Guidances](https://www.fda.gov/downloads/Drugs/GuidanceComplianceRegulatoryInformation/Guidances/UCM588857.pdf)
51 [/UCM588857.pdf](https://www.fda.gov/downloads/Drugs/GuidanceComplianceRegulatoryInformation/Guidances/UCM588857.pdf) (accessed Sep 10, 2018).
52
53
54
55
56
57 (56) Turkevich, J.; Stevenson, P. C.; Hillier, J. A Study of the Nucleation and Growth Processes in
58 the Synthesis of Colloidal Gold. *Discuss. Faraday Soc.* **1951**, *11*, 55.
59
60

- 1
2
3 (57) Zhu, J.; Yong, K.-T.; Roy, I.; Hu, R.; Ding, H.; Zhao, L.; Swihart, M. T.; He, G. S.; Cui, Y.;
4 Prasad, P. N. Additive Controlled Synthesis of Gold Nanorods (GNRs) for Two-Photon
5 Luminescence Imaging of Cancer Cells. *Nanotechnology* **2010**, *21*, 285106.
6
7
8
9
10 (58) Michen, B.; Geers, C.; Vanhecke, D.; Endes, C.; Rothen-Rutishauser, B.; Balog, S.; Petri-Fink,
11 A. Avoiding Drying-Artifacts in Transmission Electron Microscopy: Characterizing the Size and
12 Colloidal State of Nanoparticles. *Sci. Rep.* **2015**, *5*, 9793.
13
14
15
16
17 (59) Geers, C.; Rodriguez-Lorenzo, L.; Andreas Urban, D.; Kinnear, C.; Petri-Fink, A.; Balog, S. A
18 New Angle on Dynamic Depolarized Light Scattering: Number-Averaged Size Distribution of
19 Nanoparticles in Focus. *Nanoscale* **2016**, *8*, 15813–15821.
20
21
22
23
24 (60) Beltran-Villegas, D. J.; Sehgal, R. M.; Maroudas, D.; Ford, D. M.; Bevan, M. A. A
25 Smoluchowski Model of Crystallization Dynamics of Small Colloidal Clusters. *J. Chem. Phys.*
26 **2011**, *135*, 154506.
27
28
29
30
31 (61) Technologies Inc, S. Frequencies Cell Types Human Peripheral Blood
32 [https://www.stemcell.com/media/files/wallchart/WA10006-](https://www.stemcell.com/media/files/wallchart/WA10006-Frequencies_Cell_Types_Human_Peripheral_Blood.pdf)
33 [Frequencies_Cell_Types_Human_Peripheral_Blood.pdf](https://www.stemcell.com/media/files/wallchart/WA10006-Frequencies_Cell_Types_Human_Peripheral_Blood.pdf) (accessed Sep 10, 2018).
34
35
36
37
38 (62) Steiner, S.; Mueller, L.; Popovicheva, O. B.; Raemy, D. O.; Czerwinski, J.; Comte, P.; Mayer,
39 A.; Gehr, P.; Rothen-Rutishauser, B.; Clift, M. J. D. Cerium Dioxide Nanoparticles Can Interfere
40 with the Associated Cellular Mechanistic Response to Diesel Exhaust Exposure. *Toxicol. Lett.*
41 **2012**, *214*, 218–225.
42
43
44
45
46
47 (63) Administration, U. S. F. a. d. Elemental Analysis Manual (EAM) for Food and Related Products
48 <http://www.fda.gov/EAM> (accessed May 18, 2017).
49
50
51
52
53
54
55
56
57
58
59
60

For Table of Contents Only

